Time-resolved structural studies of the low-index faces of lead

J. W. Herman* and H. E. Elsayed-Ali†
Laboratory for Laser Energetics, University of Rochester, 250 East River Road, Rochester, New York 14623-1299
(Received 15 July 1993)

Reflection high-energy electron diffraction with 200-ps time resolution is used to study the structural behavior of the three low-index faces of Pb. The surfaces are subjected to heating and cooling rates on the order of 10^{11} K/s. The open Pb(110) surface is seen to reversibly disorder below the bulk melting temperature, T_m. In contrast to Pb(110), the close-packed Pb(111) surface sustains superheating to T_m+120 K. Pb(100), a surface with atomic packing intermediate to that of Pb(110) and Pb(111), shows evidence of residual order at a temperature above the bulk melting point.

I. INTRODUCTION

Although the phenomenon of melting has been studied extensively for many years, a complete understanding of the process remains elusive. It has long been speculated that melting is initiated at the surface, at a temperature below the bulk melting point, T_m.[1] A well-known relation suggests the tendency of a particular surface to melt:[2]

$$\gamma_{sv} > \gamma_{sl} + \gamma_{lv} , \quad (1)$$

where γ_{sv}, γ_{sl}, and γ_{lv} represent the interfacial free energies of the solid-vapor, solid-liquid, and liquid-vapor interfaces, respectively. This relation is valid for many surfaces at temperatures below T_m. The relation implies that, above a certain temperature, it is energetically favorable for the surface to form a thin disordered layer between the ordered solid and the vapor. This phenomenon, known as surface melting, offers an explanation for the lack of parity between supercooling and superheating.

The supercooling of melts of metals has been observed for many years.[2] Supercooling is attributed to a nucleation barrier to solidification that is a result of the competition between the decrease in free energy upon solidification and the increase in free energy that is associated with the formation of a solid-liquid interface. In the case of superheating, however, the presence of a thin disordered surface layer formed below T_m provides a vast two-dimensional site for the nucleation of melting into the bulk as T_m is approached. Therefore, for surfaces that disorder below T_m, there does not exist a nucleation barrier for melting, and this precludes substantial superheating. To form an understanding of bulk melting, extensive work has been performed examining the role of the surface in the process.[3]

One of the first conclusive experimental observations of surface melting was on Pb(110) using medium-energy ion scattering (MEIS).[4] A reversible order-disorder transformation was observed on Pb(110), with disorder beginning in the temperature range of 450–560 K, where T_m for Pb is 600.7 K. The thickness d of the disordered layer increased logarithmically beginning at 560 K ($d \sim \ln[T_m/(T_m-T)]$). At temperatures above $T_m-0.3$ K, the disordered layer thickness was observed to increase according to a power law ($d \sim [T_m-T]^{-1/3}$).[5] The functional character of the growth laws is predicted from mean-field theory.[6] Other techniques were used to study the surface melting of Pb(110).[3(b)] These techniques are complementary, and provide a coherent picture of surface melting as a continuous phase transformation. X-ray photoelectron diffraction[7] and low-energy electron diffraction (LEED) [Refs. 8(a) and 8(b)] yielded temperatures for the onset of surface disorder of 530 and 543 K, respectively. In addition, x-ray scattering,[9] UV photoelectron spectroscopy,[10] quasielastic atom scattering,[11] diffuse-light scattering,[12] and scanning tunneling microscopy[13] studies have observed surface melting on Pb(110).

To determine the role of the crystal surface orientation in the melting process, further MEIS studies were performed.[14] Pb surfaces were again studied, and the majority of the crystalline faces considered exhibited pronounced surface disordering with the exception of the vicinal surfaces within $\sim 17°$ of the {111} plane, and $\sim 10°$ of the {100} plane. The closed Pb(111) surface was observed to remain ordered up to $T_m-0.5$ K. In the MEIS experiments, the number of disordered atoms per unit area at temperatures near T_m versus surface orientation was qualitatively consistent with predictions made from surface free-energy measurements on Pb crystallites.[15] These measurements, made using electron microscopy, displayed minima in the normalized surface free energy at the {111} and {100} orientations.[15] Compared with the results from MEIS, the electron microscopy experiments predicted a significantly smaller angular region about the {100} orientation, where pronounced disorder is absent. In addition to the experiments on Pb, the importance of surface orientation was demonstrated on Al surfaces with Al(110) displaying surface melting and Al(111) remaining ordered.[16]

A recent MEIS study of Pb(111) and vicinal surfaces revealed another interesting aspect of surface melting.[17] These experiments showed that vicinals with miscut angles $\theta < 2°$ remain ordered, while vicinals with $\theta > 13.9°$ exhibited pronounced surface melting. Vicinal surfaces

0163-1829/94/49(7)/4886(12)/$06.00

with $2.0° < \theta < 13.9°$ exhibited the phenomenon of *surface-melting-induced faceting,* where the surface decomposes into "dry" and "melted" facets that coexist on the surface. In these experiments, the microscopic faceting was observed at a temperature of $T_m - 0.05$ K. In addition, the phenomenon of faceting has been observed on a macroscopic level with micrometer-sized Pb crystallites.[18,19] A theoretical treatment based on a free-energy analysis predicted the faceting behavior in these experiments.[20]

A recent MEIS study was performed on Pb(100) and its vicinal surfaces to clarify the high-temperature structural behavior of this surface, whose packing density is intermediate to that of Pb(110) and Pb(111).[21] The experiments showed that a limited amount of disorder began to form on Pb(100) at $T > 500$ K, with the degree of disorder on the considered vicinal surfaces increasing with increasing miscut angle. A logarithmic increase of the disordered layer thickness was observed on Pb(100) up to $T_m - 2$ K, where the thickness saturated at ~ 1.3 monolayers, measured up to $T_m - 0.05$ K. For the vicinal surfaces, the maximum amount of disorder was ~ 1.9 and ~ 3.5 monolayers on the 5° and 10° miscuts, respectively. The saturation of disordered layer thickness is known as *incomplete surface melting,* and is in contrast to the divergence of the disordered layer thickness on Pb(110).

The mean-field theory used by Pluis, Frenkel, and van der Veen in their MEIS study of the orientation dependence of surface melting does not account for the nondivergence of the disordered layer thickness that occurs in incomplete surface melting.[6] The role that the ordered substrate plays in the energetics of the disordered layer was recently addressed by Chernov and Mikheev.[22] In their model, the solid substrate induces a periodic density modulation in the disordered layer. The modulation is in a direction parallel to the solid-disordered layer interface. In the so-called layering model, the free energy of the disordered layer has an oscillatory character with a period of $2\pi/k_1$, where k_1 is the wave number corresponding to the first maximum in the structure factor of the bulk liquid. (For Pb, $2\pi/k_1 = 2.86$ Å.[21]) As a consequence, it becomes energetically favorable at high temperatures for the surface to form a disordered layer, with a thickness being an integral multiple of the layering period. The thickness of the disordered layer that forms in incomplete melting does not diverge as T_m is approached. This is in contrast to the behavior of Pb(110) and Al(110), which experience complete surface melting. Experimental results on the surface disordering of Ge(111),[23] Pb(100),[21] and the (100) face of the molecular crystal caprolactam[24] have been in qualitative agreement with the layering model.

Along with the experimental studies of surface melting, many molecular-dynamics (MD) studies of the structural behavior of surfaces have been conducted recently. With the development of many-body potentials, which realistically treat metallic bonding, MD studies are modeling surface-melting behavior with improved accuracy. Several fcc metals have been modeled including Al,[25–27] Au,[28–31] Cu,[32–37] Ni,[38,39] and Pb.[40] The general trend suggests that the propensity of a surface to remain ordered up to T_m is influenced by surface orientation, in agreement with experimental studies. The studies that treated the open fcc(110) surfaces demonstrated the tendency of this surface to disorder below T_m.[25,26,29,30,33–36,39] Some of these studies showed qualitative agreement with the logarithmic growth law that is evident from the experiments.[29,30,33] The disorder on the (110) surface seems to be mediated by the formation of adatom-vacancy pairs.[25,26,33–36,39] Indeed, the formation energy of a vacancy, E_v, obtained from simulations of various fcc crystalline faces, is a factor of 4 smaller for a (110) surface as compared with a (111) surface.[25] This demonstrates the tendency of the open surface to form defects. In the simulations that examined (111) surfaces, surface stability up to T_m was observed as well as superheating.[28,30,36,37,40(b)]

Surface-melting-induced faceting has also been observed in molecular-dynamics simulations. Au(111) and vicinals[31(a),31(b)] and vicinals of Pb(111) [Refs. 31(b) and 40(b)] have exhibited faceting. The study that examined Au(111) revealed that surface reconstruction plays an important role in faceting.[31(b)] At low temperatures, Au(111) has a $(23 \times 3^{1/2})$ reconstructed unit cell. In the simulations, the (534) vicinal of Au(111) was observed to facet at $0.8T_m$ as a result of surface reconstruction. In contrast to this behavior, the same vicinal of Pb(111), a surface that does not exhibit reconstruction, was free of faceting at $0.8T_m$.[31(b)]

The fcc(100) surface has been modeled less extensively.[36,38] One study that treated the low-index faces of Cu showed disordering on Cu(100) just below T_m, behavior that is qualitatively intermediate to that observed on the (110) and (111) surfaces.[36] In this study, as well as in a MD study of the high-temperature structure of vicinal surfaces of Au(100),[31(c)] stratification in the disordered layer was evident. Results of experiment and simulation suggest that the tendency of a surface to disorder below T_m depends on several factors. These include (i) the orientation-dependent surface-packing density (see Fig. 1), which influences the vibrational properties of surface atoms; (ii) the formation energy of surface defects such as adatoms and vacancies; and (iii) the ability of adatoms to diffuse on the surface.

In this study, we investigate the structural behavior of the three low-index faces of lead, using time-resolved reflection high-energy electron diffraction (RHEED). Our work is aimed at determining how the crystal surface influences the temporal dynamics of the melting process. Following a brief description of the experimental method

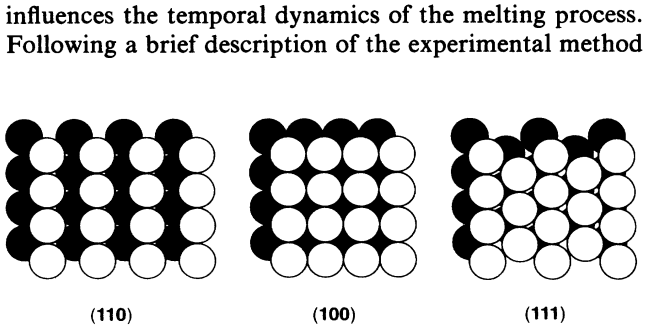

FIG. 1. The three low-index faces of a fcc metal displaying the orientation dependence of the surface packing density.

in Sec. II, we present in Sec. III results of our time-resolved structural studies of Pb(110), Pb(111), and Pb(100). The results are summarized in Sec. IV.

II. EXPERIMENT

The samples were cut from a single crystal rod aligned to within 0.75° of the appropriate orientation using Laue back reflection. The surfaces were mechanically polished prior to chemical etching in a solution of 80% glacial acetic acid and 20% hydrogen peroxide (30% in water). The samples were clipped to a resistively heated Mo stage. A thermocouple was placed between a retaining clip and the surface of the sample. The thermocouple was calibrated to the freezing and boiling points of water and to the melting point of Pb. The experiments were performed in an ultrahigh vacuum chamber with a base pressure in the low 10^{-10} range. The samples were cleaned before each experiment with cycles of Ar^+ bombardment followed by annealing. Surface cleanliness was checked using Auger-electron spectroscopy. An Auger spectrum of the clean Pb surface is shown in Fig. 2. Auger spectra were taken at an elevated temperature to ensure that no high-temperature surface impurity segregation was occurring.

The time-resolved RHEED technique will be described briefly here. It has been described in more detail elsewhere.[41] A diagram of the experimental setup is shown in Fig. 3. A Nd:YAG (yttrium aluminum garnet) laser beam ($\lambda=1.06$ μm, 200-ps pulsewidth) is split into two beams. The first is amplified, passes through an optical delay line, and strikes the surface of the sample at near-normal incidence. The second is frequency quadrupled and strikes the cathode of a photoactivated electron gun, producing electron pulses with a temporal width comparable to that of the fundamental beam. The electrons are collimated and accelerated to energies in the 15–20-keV range, and interact with the crystal in the glancing-incidence RHEED geometry, probing the first few atomic layers. Since the absorption depth of the laser into the

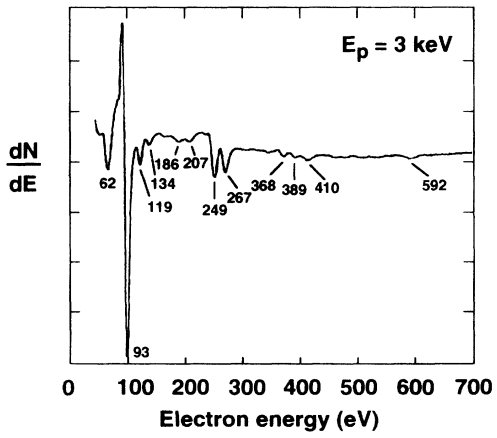

FIG. 2. Auger-electron spectrum of a clean Pb surface. The energy of the primary exciting electron beam is 3 keV. Pb peaks are labeled with the corresponding energies in electron volts. No surface impurities are detected.

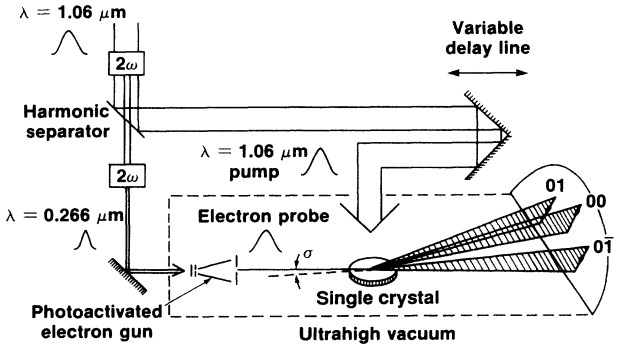

FIG. 3. Time-resolved reflection high-energy electron diffraction (RHEED). The laser pump and electron probe are synchronized on the surface of the sample. The electron beam is incident on the surface at an angle of 1°–3° with an energy typically in the 15–20-keV range.

sample (~140 Å for Pb at $\lambda=1.06$ μm) is much larger than the probed depth of the electrons (typically <5 Å), we conclude that the probed layer is essentially isothermal. The optical delay line provides the means by which the laser heating pulse and the electron probe pulse are temporally synchronized on the surface. Since the heating pulse and electron pulse originate from the same source, the system is inherently free of the timing jitter that is typically associated with electronically synchronized experiments.

Static RHEED measurements are an important component of the experiment, as they yield equilibrium surface structural information and also serve as a means to convert the time-resolved diffraction intensity to a surface-temperature rise. In this mode of operation, a Hg lamp is used to excite the cathode of the photoactivated electron gun, producing a steady electron beam. The RHEED pattern from the surface is detected by a microchannel plate (MCP) proximity focused to a phosphor screen. The resulting image is lens coupled to a linear array detector for intensity analysis. For all of the experiments reported here, the intensity of the (10) diffraction streak was measured. Line scans were taken through the center of the streak.

III. RESULTS

A. Pb(110)

The first surface studied was Pb(110),[42] which has been shown to readily disorder below T_m.[3] As an initial step to characterize the structural dynamics of Pb(110), measurements of the RHEED streak intensity versus temperature were performed. The energy of the electrons was 18.2 keV, and the beam was incident along the $\langle 1\bar{1}2\rangle$ azimuth at an angle of ~2°, resulting in a probed depth of approximately two monolayers. Results of this measurement are given in Fig. 4, where the inset is a plot of the data on a semilogarithmic scale. The intensity is seen to decay exponentially from the lowest considered temperature 487 K up to a temperature of ~520 K. This portion of the data is consistent with the Debye-Waller effect,

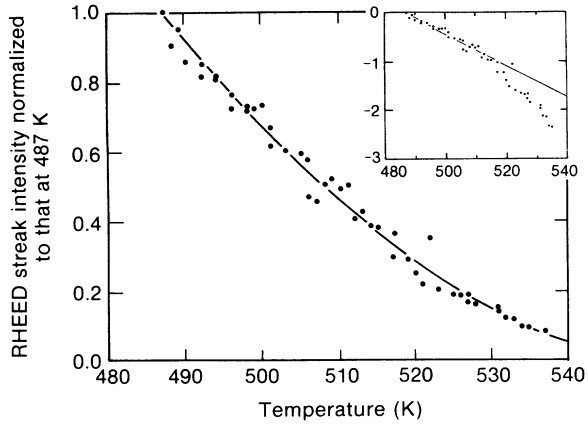

FIG. 4. RHEED streak intensity from Pb(110) normalized to that at 487 K vs temperature. A curve fit is made to the data and is used with the heat-diffusion model to obtain the predicted time-resolved modulation of the RHEED streak intensity in Fig. 5. Inset: The data are plotted on a semilogarithmic scale. The line fit includes data points up to that which maximizes the linear correlation coefficient. Note the departure from exponential Debye-Waller behavior at ~520 K.

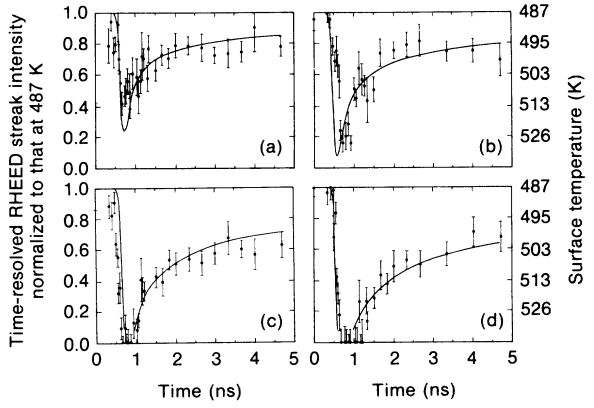

FIG. 5. Time-resolved RHEED streak intensity measurements on Pb(110). The pulse width of the laser is measured at full width at half maximum (FWHM). The corresponding surface temperature is obtained using the data of Fig. 4. (a) $I_p=1.4\times10^7$ W/cm^2, 165 ps; (b) $I_p=2.0\times10^7$ W/cm^2, 165 ps; (c) $I_p=2.7\times10^7$ W/cm^2, 175 ps; and (d) $I_p=3.6\times10^7$ W/cm^2, 170 ps. In (c) and (d) the normalized streak intensity is seen to vanish for some time, indicating that order is lost in the probed surface layer. The subsequent reappearance of the streak intensity indicates the reordering of the surface.

which predicts an exponential decay of elastic diffraction intensity with temperature. Above 520 K, the intensity is seen to deviate from Debye-Waller behavior. The initial deviation is most likely due to the anharmonic surface vibrations on Pb(110), which have been deduced from measurements of the surface expansion.[43] At higher temperatures, the deviation is attributed to surface disordering. Above $T\sim540$ K, the RHEED signal decayed into the inelastically scattered background, leading us to conclude that the probed surface layer is disordered. We therefore identify $T_d\sim540$ K as the disordering temperature of the probed layer. This behavior is qualitatively similar to that observed by Yang, Lu, and Wang on Pb(110) with high-resolution LEED.[8(c)] In their experiment, the intensity of the (00) beam at the in-phase condition departed from Debye-Waller attenuation at ~520 K.

Next we performed time-resolved measurements on Pb(110). The RHEED streak intensity, normalized to that at the sample bias temperature of 487 K, was obtained for given delay times between the arrival of the laser heating pulse and the electron probe pulse. Results are given in Fig. 5, where the solid lines represent the conversion of the temperature obtained from a one-dimensional heat-diffusion model to a normalized diffraction intensity using the static calibration of Fig. 4. The heat-diffusion model is given by

$$C\frac{dT(z,t)}{dt}=K\frac{d^2T(z,t)}{dz^2}+I_p(1-R)\alpha\exp(-\alpha z)f(t)\ , \quad (2)$$

where $T(z,t)$ is the temperature at a distance z normal to the surface ($z=0$), t is time, $C=1.58\times10^6$ J/m^3 K is the heat capacity per unit volume,[44] $K=32.2$ W/mK is the thermal conductivity,[44] $R=0.81$ is the reflectivity,[45] $\alpha=7.05\times10^7$ m^{-1} is the absorption coefficient,[45] I_p is the peak laser intensity measured in W/cm^2, and $f(t)$ represents the temporal profile of the heating pulse, which is assumed to be Gaussian.

The error bars in Fig. 5 reflect the uncertainty in the RHEED streak intensity and are primarily due to MCP noise. Other sources of error in the time-resolved experiments include the spatial nonuniformity of the laser heating, which was measured to be ±12% across the width of the sample, and the stability of the laser. The long-term laser stability was monitored throughout the experiment, and was maintained constant to within 10%. All of the time-resolved measurements presented here are the result of the convolution of the electron probe pulse with the temporal temperature profile on the surface. These convolution effects are most prominent for the times near the normalized RHEED streak intensity minimum, where the rate of change of temperature with time is greatest. Including these effects in the analysis leads to a somewhat higher peak surface temperature than what is measured. The absolute timing between the electron probe pulse and the laser heating pulse was not determined experimentally. We set the temporal position of the model with respect to the experimental data by minimizing the mean-square difference between model and experimental data for the times between 1 and 2 ns in Figs. 5(a)–5(c), and between 1.3 and 3.3 ns for Fig. 5(d). In these time intervals, convolution effects are not expected to be significant.

We next discuss the time-resolved RHEED results of Pb(110) displayed in Fig. 5. In Figs. 5(a) and 5(b), I_p is low enough not to cause any surface disordering. The surface temperature was raised from 487 K to measured peak surface temperatures of ~515 and ~530 K in Figs. 5(a) and 5(b), respectively. These are in reasonable agreement with the values of 523 and 537 K predicted by the heat-diffusion model. In Figs. 5(c) and 5(d), the peak laser intensity was increased to facilitate surface heating to temperatures above the disordering temperature T_d. In these sets, the heat-diffusion model predicted peak sur-

face temperatures of 558 (T_d+18 K) and 581 K (T_d+41 K), respectively. In both cases, the normalized RHEED streak intensity is observed to vanish for some time, indicating that the probed surface layer is disordered. The time duration over which the diffraction intensity vanishes increases from ~ 200 ps for a peak predicted temperature of T_d+18 K [Fig. 5(c)] to ~ 500 ps for a peak predicted temperature of T_d+41 K [Fig. 5(d)]. We conclude that, with the heating rate of 10^{11} K/s available from the pulsed laser, surface disordering cannot be bypassed. Furthermore, from the time-resolved data we see that the temperature at which the surface disorders is not significantly altered from that measured statically.

Subsequent to disordering, the surface recrystallizes and cools as the heat is conducted to the bulk of the sample. This is evident from the recovery of the diffraction intensity. In Figs. 5(c) and 5(d), the experimentally measured surface temperature is in accord with the model in the times where the normalized RHEED streak intensity is nonvanishing, indicating agreement with the results from heat diffusion both prior and subsequent to surface disordering. This indicates that the nucleation and growth of the disordered layer, as well as the regrowth of crystalline order, occur on a time scale less than the 180-ps pulse width of the electron probe.

The conclusion that surface disordering is a reversible process is based on static experiments where the disordered layer thickness is shown to be a distinct function of temperature, a quality that distinguishes surface disordering from bulk melting. The reversibility of surface disordering has not been previously tested for extremely high heating and cooling rates. The time-resolved results in Fig. 5 that show the recovering elastic-diffraction intensity subsequent to surface disordering indicate that surface disordering is reversible even at extremely high heating and cooling rates.

The observations of the fast regrowth of crystalline order on the time scale of the present experiment are consistent with the time scales for atomic rearrangement on Pb(110) deduced from measurements of surface mobility using He scattering.[11] The results of this experiment were described well by the following expression for the temperature-dependent mobility of surface atoms on Pb(110):[11]

$$D_s(T)=D_0\exp(-Q_s/k_BT)\ , \tag{3}$$

where $D_0=26$ cm^2/s, the activation energy of diffusion is $Q_s=0.65$ eV, k_B is Boltzmann's constant, and T is temperature. The study concluded that for $T\geq 550$ K, the mobility of surface atoms exceeds that of the bulk liquid. The above expression yields a value of ~ 0.23 Å^2/ps at $T_d\sim 540$ K, comparable to the mobility of liquid Pb close to T_m (0.22 Å^2/ps). At a temperature of T_d, over the 180-ps time scale of our electron probe, the disordered atoms diffuse over an area of ~ 40 Å^2. This area is sufficient to include all adjacent lattice sites that are potentially unoccupied. Therefore, over the time duration of the electron probe, atoms in the disordered layer have sufficient mobility to travel to adjacent lattice sites.

The time-resolved measurements on Pb(110) lead us to conclude that for heating and cooling rates on the order of 10^{11} K/s, (i) surface disordering is not bypassed, therefore precluding the existence of a nucleation barrier to disordering for these conditions; (ii) the temperature at which the surface disorders is not altered significantly from that measured statically; (iii) the nucleation and growth of surface disorder occur on a time scale less than 180 ps even for relatively small departures above T_d; and (iv) surface disordering is reversible upon cooling, even at the high rates achieved with pulsed laser heating.

B. Pb(111)

The next surface we studied was the close-packed, nonmelting Pb(111) surface, where experiments were performed to determine if the surface could be superheated.[46] The superheating of metals represents an experimental challenge and is not commonly observed. However, superheating of solids can be observed under some special conditions. Quartz and other solids that have highly viscous melts can readily be superheated.[47] This can be understood by considering the speed of propagation v of the solid-liquid interface.[48] In this treatment, v is proportional to D, the coefficient for self-diffusion in the liquid. By the Stokes-Einstein relation, D is inversely proportional to the viscosity η; thus the velocity of the solid-liquid interface is proportional to $1/\eta$. Therefore, solids that melt into highly viscous liquids are associated with extremely slow motion of the solid-liquid interface, which allows the interior of the solid to be substantially superheated.[47] Typically, melts of metals have viscosities many orders of magnitude lower than that of the previously mentioned solids. Therefore, once the surface melts, the solid-liquid interface can propagate into the bulk with velocities up to the velocity of sound in the metal.[49] However, by bypassing the melting effects of the surface, modest superheating of metals has been achieved. Preferentially cooling the surface to prevent melting,[50] coating one solid with another of higher T_m,[51] and embedding precipitates in a host metal of higher T_m (Ref. 52) are some of the methods that have been used to superheat metals. An outstanding question has been whether a surface that does not experience surface melting can be superheated. Experiments performed on *free* surfaces showed that superheating of several degrees could be observed on small metal platelets with extensive close-packed, nonmelting surfaces.[53] The experiments presented here were performed to determine if the free Pb(111) surface could be superheated to a larger degree using fast laser heating.

As with Pb(110), we first measured the RHEED streak intensity versus temperature. The angle of incidence of the 18.2-keV electron beam was $\sim 2°$, leading to a probed depth of two monolayers. The electron beam was incident along the $\langle 01\bar{1}\rangle$ azimuth. Results of this measurement are shown in Fig. 6, where the RHEED streak intensity is normalized to that at 407 K, and the inset is plotted on a semilogarithmic scale. It is apparent that the behavior of Pb(111) is qualitatively different from that of Pb(110) shown in Fig. 4, where deviation from Debye-Waller behavior occurred at $\sim T_m-80$ K. With Pb(111),

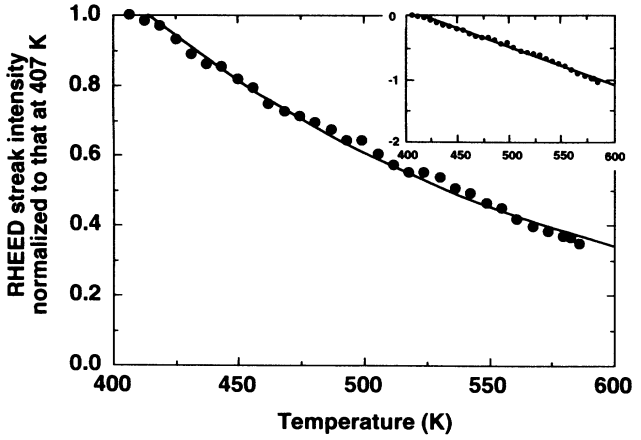

FIG. 6. RHEED streak intensity of Pb(111), normalized to that at 407 K, vs sample temperature. An exponential curve fit has been made to the data. Inset: The data plotted on a semilogarithmic scale showing Debye-Waller behavior up to $T_m - 15$ K.

the RHEED streak intensity is seen to decay exponentially in the considered temperature range extending to $T_m - 15$ K. This is consistent with the Debye-Waller effect, and agrees qualitatively with the results from MEIS, where Pb(111) was shown to remain ordered up to $T_m - 0.5$ K.[14]

In the next set of experiments, Pb(111) was subjected to laser pulses with $I_p \sim 3.3 \times 10^7$ W/cm^2, while the sample bias temperature T_{bias} was raised from 495 to 575 K. The RHEED streak intensity, normalized to that at T_{bias}, is shown in Fig. 7(a) for the time corresponding to the minimum of the diffraction intensity, t_0. (The time t_0 is temporally close to the time corresponding to the peak of the surface-temperature rise. These times do not coincide due to the effects of convolution.) The diffraction intensity is observed to decrease linearly with T_{bias}. No sudden decrease in diffraction intensity is observed that would indicate a phase transformation taking place on the surface. The diffraction intensity is converted to a temperature jump ΔT by utilizing the static RHEED measurement of Fig. 6. The result of this conversion is shown in Fig. 7(b), where for $T_{\text{bias}} \geq 530$ K, the peak surface temperature $T_{\text{bias}} + \Delta T$ exceeds T_m, and the surface is superheated. It is observed that ΔT increases linearly with T_{bias}. This reflects the changing optical and thermal properties of the sample in the temperature range considered. The change in surface reflectivity R with temperature is a significant factor in the increase of ΔT with T_{bias} since the absorption of laser energy at the surface is proportional to $1-R$. The reflectivity of the surface at the heating laser wavelength was measured directly and found to decrease from 0.78 to 0.74 in the temperature range of Fig. 7. The results from a solution of the heat-diffusion model are shown in Fig. 7(b) as well. The larger ΔT predicted by the model is due to the above-mentioned convolution effects, which lead to a somewhat lower experimentally measured surface-temperature rise. In addition, the increase in ΔT with increasing T_{bias} was observed at delay times subsequent to t_0; these results are given in Fig. 8. For a given T_{bias} we observe a decrease in ΔT with increasing delay time. This reflects the cooling of the surface after the arrival of the heating laser pulse.

Further experiments were performed to determine the magnitude of superheating that could be sustained on Pb(111). The sample was biased at $T_{\text{bias}} = 586$ K ($T_m - 15$ K) and transiently heated with varying peak laser intensities. The RHEED streak intensity normalized to that at T_{bias} was obtained at given times throughout the laser-heating process. Such a set is shown in Fig. 9. This set was performed at the time t_0. The inset of Fig. 9 is the data plotted on a semilogarithmic scale. Two regimes are evident: the first, where $I_p < 3.5 \times 10^7$ W/cm^2 shows an exponential decay of the diffraction intensity with I_p, consistent with Debye-Waller behavior; in the second regime, where $I_p \geq 3.5 \times 10^7$ W/cm^2, we observe a marked deviation from exponential behavior, indicating that melting is occurring on the surface.

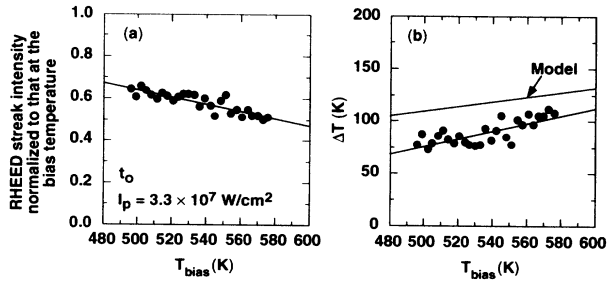

FIG. 7. (a) Modulation of the normalized RHEED streak intensity for $I_p \sim 3.3 \times 10^7$ W/cm^2 and varying sample bias temperatures T_{bias}. This data set was obtained at the time corresponding to the temporal minimum of the normalized streak intensity, t_0. (b) The streak intensity of (a) is converted to a peak surface-temperature rise ΔT, using the data of Fig. 6. Results from the heat-diffusion model are plotted as well. The higher ΔT predicted by the model is due to convolution effects that are most prominent at t_0. For $T_{\text{bias}} \geq 530$ K, the peak surface temperature exceeds T_m.

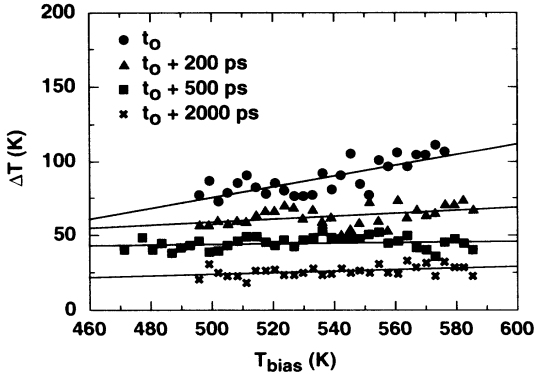

FIG. 8. Surface-temperature rise vs T_{bias} for $I_p \sim 3.3 \times 10^7$ W/cm^2 performed at t_0 and subsequent delay times. The general trend of increasing ΔT with T_{bias} is attributed to the change in optical and thermal properties of the sample in the temperature range considered.

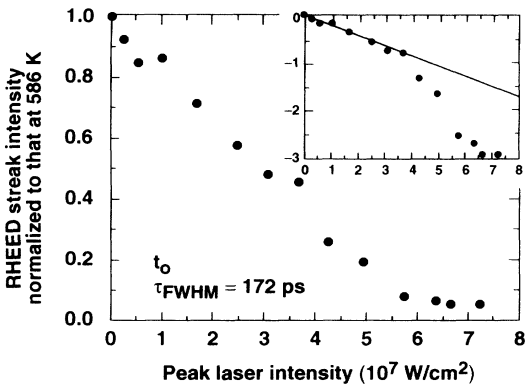

FIG. 9. RHEED streak intensity normalized to that at 586 K vs peak laser intensity. This data set was performed at t_0. Inset: A plot of the data on a semilogarithmic scale showing deviation from Debye-Waller behavior at $I_p \sim 3.5\times10^7$ W/cm^2. The corresponding peak surface temperature is $\sim T_m + 120$ K.

We next estimate the temperature at which deviation from exponential, Debye-Waller behavior occurs, and identify this as the peak observed superheating temperature. To accomplish this, we consider diffraction intensity modulations for small I_p such that the corresponding temperature jumps ΔT lead to peak temperatures below T_m. In the Debye-Waller region, $\Delta T \propto I_p$; therefore, lower values of I_p can be used to make a correspondence between I_p and peak surface temperature. When this is done, we conclude that deviation from Debye-Waller behavior occurs at a temperature of $\sim$720 K ($\sim T_m + 120$ K). Furthermore, the time-resolved diffraction data have a slope when plotted on a semilogarithmic scale that is equivalent to the slope from the static RHEED measurement of Fig. 6, within experimental error. This error can result from the fact that this experiment was performed at the time t_0 where convolution effects can be prominent. The exponential dependence of the normalized RHEED streak intensity up to $T_m + 120$ K indicates that the surface retains order above T_m, and behaves according to the Debye-Waller effect with mean-square vibrational amplitudes in excess of that at T_m.

The time-resolved measurements of the diffraction intensity versus I_p were carried out at other times relative to the time t_0. Figure 10 shows measurements performed at $t_0 + 500$ ps and $t_0 + 4000$ ps. The insets are plotted on a semilogarithmic scale. In both cases, for $I_p < 3.5\times10^7$ W/cm^2 we observe an exponential decrease in diffraction intensity with increasing I_p, as is evident from the linear behavior in the insets. A distinct break from exponential behavior occurs at $I_p \geq 3.5\times10^7$ W/cm^2, consistent with the value obtained at the time t_0. We conclude that this deviation from Debye-Waller behavior is due to melting taking place on the surface. This deviation, at $I_p \geq 3.5\times10^7$ W/cm^2, is most likely not attributed to anharmonic vibrations due to the observed deviation from exponential behavior at $t_0 + 4000$ ps, an amount of time after t_0 where such vibrations should not be present due to the rapid decrease of the surface temperature rise.

Similar measurements were performed with the electron beam incident at an angle of $\sim 1°$ with respect to the surface. This led to a probed depth of less than a monolayer. Plots of the RHEED streak intensity normalized to that at 586 K are shown in Fig. 11 for the times t_0 and $t_0 + 4000$ ps. A break from exponential Debye-Waller behavior is seen to occur at $I_p \sim 3$–4×10^7 W/cm^2, consistent with what was observed for the previous data with an angle of incidence of $\sim 2°$.

Time-resolved experiments examining the RHEED streak intensity throughout the heating process were carried out with $T_{bias} = 586$ K. The RHEED streak intensity, normalized to that at 586 K, was obtained at various delay times. Results for varying I_p are shown in Fig. 12. Figure 12(a) exhibits the qualities of classical heat diffusion: a rapid decrease in the normalized streak intensity followed by an increase as the heat is conducted to the bulk of the sample. The data set of Fig. 12(a) was normalized to sets taken at lower T_{bias}, which corresponded to peak temperatures below T_m. This comparison showed good agreement, indicating that the data of Fig. 12(a) are consistent with classical heat diffusion. Since the time-resolved RHEED streak intensity at $T_{bias} = 586$ K exhibited Debye-Waller behavior up to $I_p \sim 3.5\times10^7$ W/cm^2, the static RHEED calibration of Fig. 6 can be used to determine the peak ΔT of Fig. 12(a). When this is done, a peak surface temperature of $T_m + 110$ K is deduced.

In Figs. 12(b)–12(d), the surface was subjected to $I_p > 3.5\times10^7$ W/cm^2, the threshold for Debye-Waller behavior. We observe a clear deviation from classical heat diffusion in the tail after ~ 1.5 ns. The streak intensity, subsequent to an initial fast rise at t_0, fails to recover

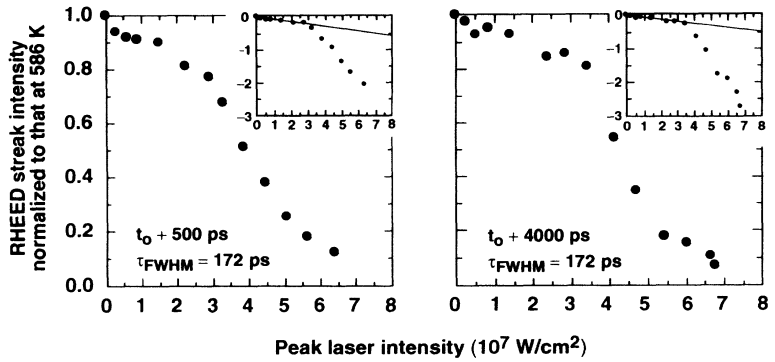

FIG. 10. RHEED streak intensity normalized to that at 586 K vs peak laser intensity. These sets were performed at times of $t_0 + 500$ ps and $t_0 + 4000$ ps. The insets are plotted on a semilogarithmic scale, and show the break from Debye-Waller behavior at $I_p \sim 3$–4×10^7 W/cm^2, consistent with what was observed at the time t_0.

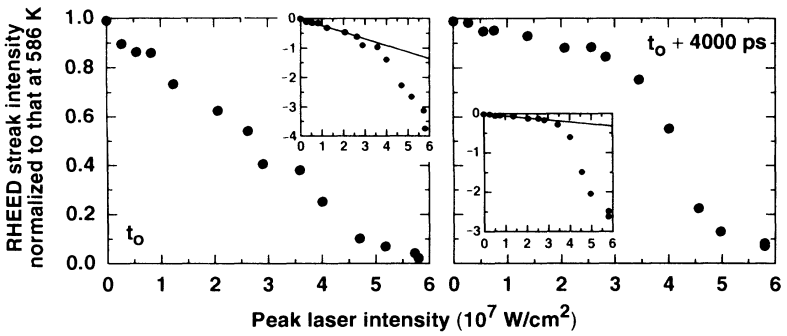

FIG. 11. RHEED streak intensity normalized to that at 586 K vs peak laser intensity for an electron-beam angle of incidence of $\sim 1°$ at the times t_0 and t_0+4000 ps. Insets show the departure from Debye-Waller behavior at $I_p \sim 3-4\times 10^7$ W/cm^2.

to what is expected from heat diffusion. The behavior at times after t_0 is also reflected in the data of Fig. 10. We attribute this to melting on part of the surface. In Figs. 12(b)–12(d), the value of the normalized streak intensity at times after t_0 depends on the ratio of the molten portion of the probed surface area to that which remains solid. This in turn is influenced by the spatial intensity profile of the laser pulse on the sample surface. In these experiments, the laser nonuniformity was measured to be $\pm 18\%$ across the width of the sample. This was accomplished by measuring the laser intensity passing through a small pinhole that was scanned through the beam. This measurement, however, does not preclude the existence of laser nonuniformities on a micrometer scale. Laser-intensity variations on this scale could influence the dynamics of the melting process.

We define the time τ to be the time interval between t_0 and the time at which the diffraction intensity deviates from behavior consistent with classical heat diffusion. To determine τ, a nonmelting superheated set was normalized to a given melting set and subtracted from it. The difference that resulted was fitted with a polynomial that was differentiated to observe the break from nonmelting behavior. A plot of τ versus peak laser intensity is given in Fig. 13 for data sets biased at 586 K. The time τ is observed to decrease from 1200 to <300 ps for $I_p \sim 3.8\times 10^7$ W/cm^2 to $I_p \sim 6.0\times 10^7$ W/cm^2, respectively.

From the experiments on Pb(111), we conclude that this surface, which exhibits no surface melting, sustains superheating to $\sim T_m + 120$ K. This is evident from the exponential Debye-Waller behavior of the RHEED streak intensity in this temperature range. In the superheating regime, the excess surface temperature is manifested as lattice mean-square vibrational amplitudes exceeding that at T_m. Melting is apparently bypassed by the 10^{11}-K/s heating and cooling rates available with pulsed laser heating. At incident peak laser intensities greater than $\sim 3.5\times 10^7$ W/cm^2, the surface melts, as is evident from the pronounced deviation from Debye-Waller behavior. The larger heating rates available with lasers of shorter pulse width could conceivably lead to a larger degree of superheating.

As an interesting postscript to the experiments on Pb(111), recent molecular-dynamics simulations were performed by Häkkinen and Landman examining the dynamics of melting and superheating of Cu surfaces.[37] Motivated by the time-resolved laser heating experiments, they constructed a model that incorporated ener-

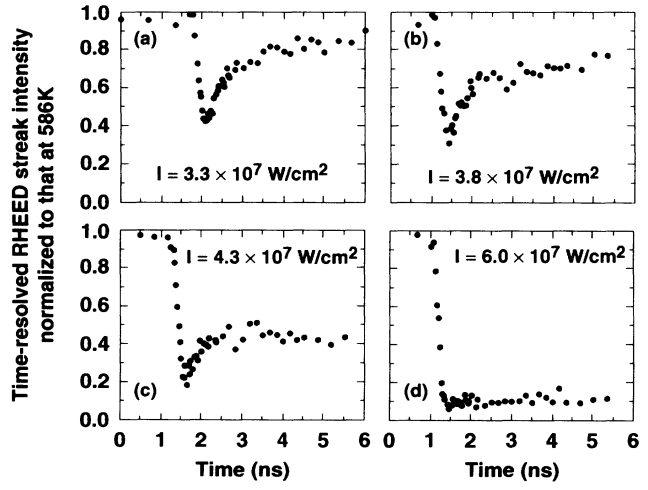

FIG. 12. Time-resolved normalized RHEED streak intensity of Pb(111) irradiated with laser pulses of varying peak intensity. Set (a) is consistent with classical heat diffusion and corresponds to a peak surface temperature of $T_m + 110$ K. In sets (b)–(d), where $I_p \geq 3.5\times 10^7$ W/cm^2, the surface begins to melt, as is evident from the pronounced deviation from classical heat diffusion.

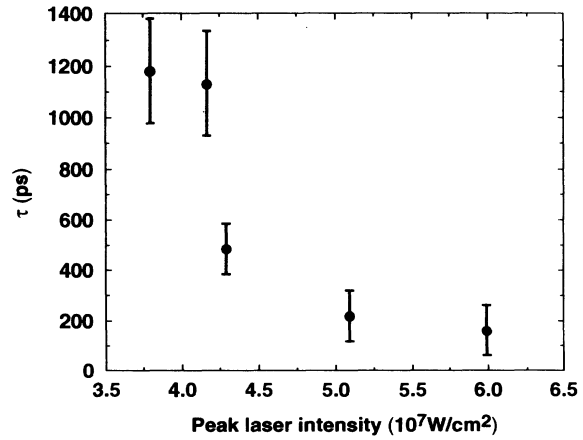

FIG. 13. The time interval τ, from t_0 to the time at which deviation from classical heat diffusion occurs, is extracted from data sets as in Figs. 12(b) and 12(c). The time τ is seen to decrease with increasing peak laser intensity.

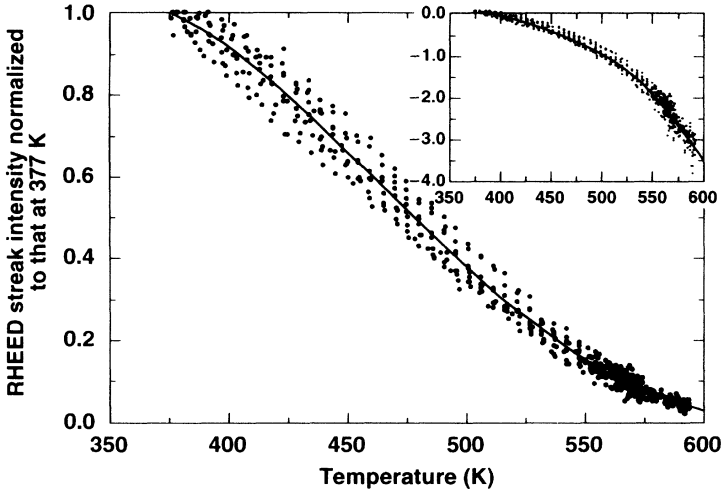

FIG. 14. RHEED streak intensity from Pb(100) normalized to that at 377 K vs temperature. The inset shows the data plotted on a semilogarithmic scale. The solid lines are polynomial fits to the data. The streak intensity is observed to deviate from Debye-Waller behavior for $T \geq 475$ K.

gy transfer from the electronic system to the lattice. The subsequent lattice dynamics were modeled with the many-body embedded-atom potential. They observed rapid and reversible disordering of the Cu(110) surface, in analogy to Pb(110). In contrast to this, Cu(111) was shown to sustain superheating of 40 K. Further simulations focused on the effects of defects in the superheating process.[37] Defects such as steps and vacancies are expected to be present on any metal surface in experimental situations. The simulations showed that even highly defected Cu(111) surfaces, with up to a 10% initial surface vacancy concentration, sustained substantial superheating. A settling mechanism involving adatoms was observed in the annealing process that acted to fill existing vacancies and restore crystalline order. Processes such as this may be involved in the time-resolved experiments on Pb(111), where a large degree of superheating was sustained.

C. Pb(100)

The final surface considered was Pb(100),[54] which has been shown to experience incomplete surface melting. Using MEIS, it was observed that the disordered layer that forms on the surface does not nucleate further melting up to a temperature of $T_m - 0.05$ K.[21] The aim of our time-resolved experiments on Pb(100) was to determine if the disordered layer that forms on the surface is stable at temperatures above T_m. The first experiment on Pb(100) measured the temperature dependence of the RHEED streak intensity. The 15-keV electron beam was incident along the ⟨001⟩ azimuth at an angle of 3°, resulting in a probed depth of ~5 Å. This corresponds to ~3 monolayers. A plot of the RHEED streak intensity normalized to that at 377 K is shown in Fig. 14. The inset is a plot of the data on a semilogarithmic scale. A nonexponential decrease in diffraction intensity with temperature is observed starting at a temperature of ~475 K. The data are qualitatively similar to that obtained on Pb(100) by Yang *et al.* using high-resolution LEED.[55] The deviation from Debye-Waller behavior may be related initially to the surface expansion that they observed between 300 and 470 K. In this temperature range, the surface undergoes an expansion exceeding that of the bulk by a factor of 7. This surface expansion is directly related to the anharmonic nature of the surface interatomic potential. In addition, deviation from Debye-Waller behavior can be attributed to the abrupt increase in vacancy concentration observed beginning at 510 K.[55]

To determine the peak temperature rise induced on the Pb(100) surface by the heating laser pulse, time-resolved measurements were performed at the time t_0. For these experiments, the sample was biased at temperatures of 450 and 533 K. The RHEED streak intensity, normalized to that at 450 K, is shown in Fig. 15 for various peak laser intensities I_p. The normalized streak intensity is converted to a temperature rise ΔT, using the calibration of Fig. 14. The result of this conversion is shown in the inset of Fig. 15, where ΔT is plotted versus I_p. The temperature rise is observed to be directly proportional to I_p, which is consistent with classical heat diffusion. The maximum peak temperature in all of these sets is below T_m. These data do not account for the effect of convolution.

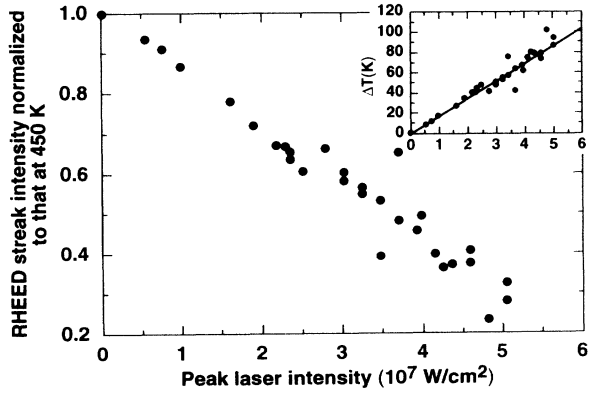

FIG. 15. RHEED streak intensity vs peak laser intensity on Pb(100) at the time t_0. The sample was biased at 450 K. Inset: Peak surface temperature rise ΔT vs I_p. The inset is a result of the conversion of the streak intensity modulation to a ΔT using the data of Fig. 14. These data are used to determine ΔT for RHEED measurements with T_{bias} closer to T_m.

In the next set of experiments the RHEED streak intensity, normalized to that at a given T_{bias}, is obtained for various I_p. In these experiments, performed at t_0, T_{bias} is raised closed to T_m. Results are shown in Fig. 16, where the set in Fig. 16(d) is biased just 11 K below T_m. At sufficiently high I_p, the normalized streak intensity is observed to vanish, indicating that order has been lost in the probed surface layer. The value of I_p necessary to disorder the probed surface layer decreases from $\sim 4.3\times10^7$ W/cm^2 for $T_{bias}=533$ K to $\sim 1.8\times10^7$ W/cm^2 for $T_{bias}=590$ K. The data of Fig. 15 are used to determine the peak surface temperature at which the normalized RHEED streak intensity vanishes. In each of the sets of Fig. 16, the lowest I_p leading to a vanishing RHEED streak intensity is converted to a temperature rise using Fig. 15. From this conversion, we see that the peak surface temperature $T_{bias}+\Delta T$, when order is lost in the probed surface layer, is $\sim 615+20$ K. The error accounts for (i) the spread of the static RHEED data; (ii) the spread of the temperature-rise data of Fig. 15; and (iii) the nonuniformity of laser heating, which was measured to be $\pm 25\%$ over the entire width of the sample. Factors not accounted for in this peak temperature include convolution effects and the changes in the thermal and optical properties of the sample occurring over the considered temperature range. These effects lead to a somewhat greater peak surface temperature than what is experimentally observed.

The temporal behavior of the heating and disordering process on Pb(100) was examined using time-resolved RHEED. In Fig. 17, results are given for varying sample bias temperatures and incident peak laser intensities. In Figs. 17(a) and 17(b), the incident peak laser intensity was not sufficient to cause disorder in the probed layer. This is evident by the nonvanishing diffraction intensities in these sets. In Fig. 17(c), sufficient laser intensity was provided to disorder the probed surface layer. The disordering is evident from the vanishing streak intensity at time

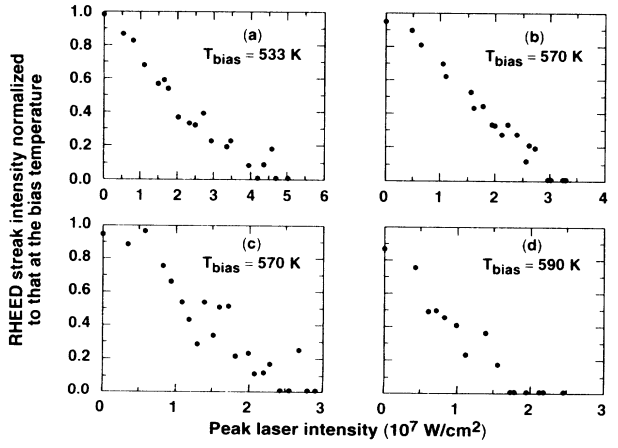

FIG. 16. Normalized RHEED streak intensity vs peak laser intensity for T_{bias} successively closer to T_m. The streak intensity vanishes for I_p above a certain threshold depending on T_{bias}. This threshold is used along with the data of Fig. 15 to determine the temperature at which order is lost in the probed layer.

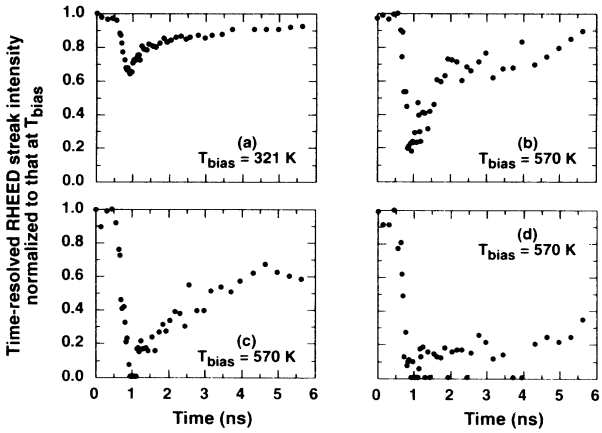

FIG. 17. Time-resolved normalized RHEED streak intensity on Pb(100) at different bias temperatures, subjected to varying peak laser intensities. (a) $T_{bias}=321$ K, $I_p=4.4\times10^7$ W/cm^2; (b) $T_{bias}=570$ K, $I_p=2.3\times10^7$ W/cm^2; (c) $T_{bias}=570$ K, $I_p=3.4\times10^7$ W/cm^2; and (d) $T_{bias}=570$ K, $I_p=5.1\times10^7$ W/cm^2.

~ 1 ns. Subsequent to disordering, the surface recrystallizes and cools, as is seen from the increasing streak intensity at later times. Finally, in Fig. 17(d), the streak intensity fails to recover for times ≥ 4 ns after the initial disordering, which is an indication of melting on the surface. In these experiments, no surface damage was visible upon recrystallization.

From our experiments on Pb(100) we conclude that residual order is present on Pb(100) at a peak surface temperature of 615 ± 20 K. Considering the previously mentioned convolution effects, it is likely that residual order is present above T_m. At this temperature the surface is most likely proliferated with defects such as vacancies.[55] The degree of superheating would undoubtedly be lowered by the presence of vacancies. Compared with Pb(111), where superheating to ~ 720 K was observed,[46] Pb(100) shows evidence of residual order at a much lower surface temperature. Our experiments show that the disordered layer that forms near T_m is stable in a narrow temperature range *above* T_m. Evidently, in this temperature range a second layering transition is not energetically favorable. Above the observed peak surface temperature, further disordering occurs and the residual order in the probed layer vanishes. At this temperature, a second layer transition may take place increasing the disordered layer thickness to $4\pi/k_1\sim 5.7$ Å, exceeding the 5 Å probed by our electron beam.

IV. SUMMARY

From our experimental results on the low-index faces of Pb, we conclude that the time-resolved surface structural behavior of Pb has a pronounced orientation dependence. The open Pb(110) surface was seen to disorder rapidly and reversibly with the 10^{11}-K/s heating and cooling rates available from pulsed laser heating. It is likely that higher index planes, which were shown to exhibit surface disordering in the case of Pb,[14] would exhib-

it rapid disordering analogous to that observed on Pb(110). In contrast, the close-packed Pb(111) surface, which was shown not to experience surface melting,[14] exhibited Debye-Waller behavior upon laser heating up to $\sim T_m + 120$ K. We are not aware of any larger superheating of a free metal surface; however, greater superheating may be possible with larger heating rates. In addition, the nonmelting (0001) face of Bi was shown to exhibit substantial superheating using time-resolved RHEED.[56] The last surface we studied was Pb(100), a surface that exhibits incomplete surface melting. Pb(100) showed residual order up to $\sim 615 \pm 20$ K, a result that differs from that obtained on Pb(111) in two respects. First, the diffraction intensity from Pb(100) deviated from Debye-Waller behavior at $T \sim 475$ K, unlike Pb(111), which upon laser heating showed Debye-Waller behavior up to $T \sim 720$ K.[46] It is likely that Pb(100) develops a high concentration of surface defects at temperatures above 500 K.[55] Second, the temperature at which order is completely lost on Pb(100) is much lower than that of Pb(111). The disordered layer that forms on Pb(100) at elevated temperatures precludes substantial excursions above T_m. However, our time-resolved experiments show that residual order on Pb(100) is preserved for *small* excursions above T_m. This implies that there is a barrier for the growth of the disordered layer thickness on Pb(100) at temperatures above T_m.

ACKNOWLEDGMENTS

This work was supported by the U.S. Department of Energy under Contract No. DE-FG02-88ER45376. We gratefully acknowledge E. A. Murphy for her assistance with the experiments.

*Also at the Department of Physics and Astronomy, University of Rochester, Rochester, NY 14627.

†Present address: Department of Electrical and Computer Engineering, Old Dominion University, Norfolk, VA 23529.

[1]M. Faraday, Proc. R. Soc. London **10**, 440 (1860); G. Tammann, Z. Phys. Chem. **72**, 609 (1910).

[2]D. P. Woodruff, *The Solid-Liquid Interface* (Cambridge University Press, London, 1973).

[3](a) J. F. van der Veen, B. Pluis, and A. W. Denier van der Gon, in *Chemistry and Physics of Solid Surfaces VII,* edited by R. Vanselow and R. F. Howe (Springer-Verlag, Berlin, 1988), p. 455; (b) J. W. M. Frenken, J. Vac. Sci. Technol. A **7**, 2147 (1989).

[4]J. W. M. Frenken and J. F. van der Veen, Phys. Rev. Lett. **54**, 134 (1985); J. W. M. Frenken, P. M. J. Maree, and J. F. van der Veen, Phys. Rev. B **34**, 7506 (1986).

[5]B. Pluis, T. N. Taylor, D. Frenkel, and J. F. van der Veen, Phys. Rev. B **40**, 1353 (1989).

[6]B. Pluis, D. Frenkel, and J. F. van der Veen, Surf. Sci. **239**, 282 (1990).

[7]U. Breuer, O. Knauff, and H. P. Bonzel, Phys. Rev. B **41**, 10 848 (1990); J. Vac. Sci. Technol. A **8**, 2489 (1990).

[8](a) K. C. Prince, U. Breuer, and H. P. Bonzel, Phys. Rev. Lett. **60**, 1146 (1988); (b) U. Breuer, H. P. Bonzel, K. C. Prince, and R. Lipowsky, Surf. Sci. **223**, 258 (1989); (c) H.-N. Yang, T.-M. Lu, and G.-C. Wang, Phys. Rev. Lett. **63**, 1621 (1989).

[9]P. H. Fuoss, L. J. Norton, and S. Brennan, Phys. Rev. Lett. **60**, 2046 (1988); B. Pluis, J. M. Gay, J. W. M. Frenken, S. Gierlotka, J. F. van der Veen, J. E. MacDonald, A. A. Williams, N. Piggins, and J. Als-Nielsen, Surf. Sci. **222**, L845 (1989).

[10]P. Thiry, F. Jezequel, and Y. Petroff, J. Vac. Sci. Technol. A **5**, 892 (1987).

[11]J. W. M. Frenken, J. P. Toennies, and Ch. Wöll, Phys. Rev. Lett. **60**, 1727 (1988).

[12]H.-N. Yang, K. Fang, T.-M. Lu, and G.-C. Wang, Phys. Rev. B **47**, 15 842 (1993).

[13]L. Kuipers and J. W. M. Frenken, Phys. Rev. Lett. **70**, 3907 (1993).

[14]B. Pluis, A. W. Denier van der Gon, J. F. van der Veen, and A. J. Riemersma, Surf. Sci. **239**, 265 (1990).

[15]J. C. Heyraud and J. J. Métois, Surf. Sci. **128**, 334 (1983).

[16]A. W. van der Gon, R. J. Smith, J. M. Gay, D. J. O'Connor, and J. F. van der Veen, Surf. Sci. **227**, 143 (1990).

[17]H. M. van Pinxteren and J. W. M. Frenken, Europhys. Lett. **21**, 43 (1993).

[18]J. C. Heyraud, J. J. Métois, and J. M. Bermond, J. Cryst. Growth **98**, 355 (1989).

[19]A. Pavlovska, K. Faulian, and E. Bauer, Surf. Sci. **221**, 233 (1989).

[20]P. Nozières, J. Phys. France **50**, 2541 (1989).

[21]H. M. van Pinxteren and J. W. M. Frenken, Surf. Sci. **275**, 383 (1992).

[22]A. A. Chernov and L. V. Mikheev, Phys. Rev. Lett. **60**, 2488 (1988); Physica A **157**, 1042 (1989).

[23]A. W. Denier van der Gon, J. M. Gay, J. W. M. Frenken, and J. F. van der Veen, Surf. Sci. **241**, 335 (1991).

[24]S. Chandavarkar, R. M. Geertman, and W. H. de Jeu, Phys. Rev. Lett. **69**, 2384 (1992).

[25]P. Stoltze, J. K. Nørskov, and U. Landman, Phys. Rev. Lett. **61**, 440 (1988); Surf. Sci. **220**, L693 (1989).

[26]P. Stoltze, J. Chem. Phys. **92**, 6306 (1990).

[27]J. Mei and J. W. Davenport, Phys. Rev. B **46**, 21 (1992).

[28]P. Carnevali, F. Ercolessi, and E. Tosatti, Phys. Rev. B **36**, 6701 (1987); Surf. Sci. **189/190**, 645 (1987).

[29]F. Ercolessi, S. Iarlori, O. Tomagnini, E. Tosatti, and X. J. Chen, Surf. Sci. **251/252**, 645 (1991).

[30]F. Ercolessi, O. Tomagnini, S. Iarlori, and E. Tosatti, in *Manipulation of Atoms in High Fields and Temperatures: Applications, NATO Advanced Study Institute, Series E: Applied Sciences,* edited by Vu Thien Binh, N. Garcia, and K. Dransfeld (Kluwer Academic, Dordrecht, 1992).

[31](a) G. Bilalbegović, F. Ercolessi, and E. Tosatti, Surf. Sci. Lett. **258**, L676 (1991); (b) Europhys. Lett. **18**, 163 (1992); (c) Surf. Sci. **280**, 335 (1993).

[32]J. F. Lutsko, D. Wolf, S. R. Phillpot, and S. Yip, Phys. Rev. B **40**, 2841 (1989).

[33]R. N. Barnett and U. Landman, Phys. Rev. B **44**, 3226 (1991).

[34]P. D. Ditlevsen, P. Stoltze, and J. K. Nørskov, Phys. Rev. B **44**, 13 002 (1991).

[35]B. Loisel, J. Lapujoulade, and V. Pontikis, Surf. Sci. **256**, 242 (1991).

[36]H. Häkkinen and M. Manninen, Phys. Rev. B **46**, 1725 (1992).

[37]H. Häkkinen and U. Landman, Phys. Rev. Lett. **71**, 1023 (1993).

[38]E. T. Chen, R. N. Barnett, and U. Landman, Phys. Rev. B **40**, 924 (1989).

[39]E. T. Chen, R. N. Barnett, and U. Landman, Phys. Rev. B **41**, 439 (1990).

[40](a) P. Tibbits, M. Karimi, D. Ila, I. Dalins, and G. Vidali, J. Vac. Sci. Technol. A **9**, 1937 (1991); (b) G. Bilalbegović, F. Ercolessi, and E. Tosatti, Europhys. Lett. **17**, 333 (1992).

[41]H. E. Elsayed-Ali and G. A. Mourou, Appl. Phys. Lett. **52**, 103 (1988); H. E. Elsayed-Ali and J. W. Herman, Rev. Sci. Instrum. **61**, 1636 (1990).

[42]J. W. Herman and H. E. Elsayed-Ali, Phys. Rev. Lett. **68**, 2952 (1992).

[43]J. W. M. Frenken, F. Huussen, and J. F. van der Veen, Phys. Rev. Lett. **58**, 401 (1987).

[44]*Thermophysical Properties of Matter,* edited by Y. S. Toukoukian (Plenum, New York, 1970), Vols. 1 and 4.

[45]From $R=[(n-1)^2+k^2]/[(n+1)^2+k^2]$ and $\alpha=4\pi k/\lambda$, where n and k are the real and imaginary parts of the complex index of refraction. The values of n and k are obtained from an interpolation of the data in A. I. Golovashkin and G. P. Motulevich, Zh. Eksp. Teor. Fiz. **53**, 1526 (1967) [Sov. Phys. JETP **26**, 881 (1968)].

[46]J. W. Herman and H. E. Elsayed-Ali, Phys. Rev. Lett. **69**, 1228 (1992).

[47]N. G. Ainslie, J. D. MacKenzie, and D. Turnbull, J. Phys. Chem. **65**, 1718 (1961); R. L. Cormia, J. D. MacKenzie, and D. Turnbull, J. Appl. Phys. **34**, 2239 (1963); D. R. Uhlmann, J. Non-Cryst. Solids **41**, 347 (1980).

[48]D. Turnbull and M. H. Cohen, in *Modern Aspects of the Vitreous State,* edited by J. D. MacKenzie (Butterworths, London, 1960), Vol. 1.

[49]C. A. MacDonald, A. M. Malvezzi, and F. Spaepen, J. Appl. Phys. **65**, 129 (1989).

[50]S. E. Kaykin and N. P. Bene, C. R. Acad. Sci. USSR **23**, 31 (1939).

[51]J. Daeges, H. Gleiter, and J. H. Perepezko, Phys. Lett. A **119**, 79 (1986).

[52]L. Gråbaek, J. Bohr, E. Johnson, A. Johansen, L. Sarholt-Kristensen, and H. H. Andersen, Phys. Rev. Lett. **64**, 934 (1990).

[53]S. J. Peppiatt, Proc. R. Soc. London Ser. A **345**, 401 (1975); G. D .T. Spiller, Philos. Mag. A **46**, 535 (1982); J. J. Métois and J. C. Heyraud, J. Phys. (Paris) **50**, 3175 (1989).

[54]J. W. Herman, H. E. Elsayed-Ali, and E. A. Murphy, Phys. Rev. Lett. **71**, 400 (1993).

[55]H.-N. Yang, K. Fang, G.-C. Wang, and T.-M. Lu, Phys. Rev. B **44**, 1306 (1991).

[56]E. A. Murphy, H. E. Elsayed-Ali, and J. W. Herman, Phys. Rev. B **48**, 4921 (1993).